POSITRON RING CAMERAS FOR EMISSION-COMPUTED TOMOGRAPHY

Stephen E. Derenzo
Donner Laboratory
University of California
Berkeley, California 94720

ABSTRACT

A properly designed circular ring of NaI(Tl) crystals and suitable reconstruction algorithms can provide rapid, high-resolution transverse section images of positron-labeled compounds in the human body. The spatial resolution is limited by the crystal center-to-center spacing and by the positron range in tissue. Using 280 crystals with 10-mm center-to-center spacing and isotopes such as ^{68}Ga, ^{11}C, ^{18}F, or ^{52}Fe, a resolution of 7.5 mm full width at half maximum (FWHM) is possible. Improvements in this technology will involve larger numbers of smaller crystals, more efficient crystals (possibly bismuth germanate), or faster detectors (such as loaded organic scintillators).

1. INTRODUCTION

The first camera specifically designed to produce transverse section images of positron-labeled compounds in the human body was built by Rankowitz, Robertson, and co-workers at Brookhaven National Laboratory in 1962.[1,2] This innovative instrument employed 32 NaI(Tl) detectors in a circular pattern and was built about 10 years before the mathematical techniques for accurate tomographic reconstruction had been developed.[3] It is now in use at the Montreal Neurological Institute.[4,5]

More recently, a 48-crystal hexagonal system has been built by Ter-Pogossian and co-workers at Washington University at St. Louis[6-10] and a 64-crystal ring system has been built by Cho and co-workers at UCLA.[11-13] In addition, the planar detector positron camera systems of Brownell[14,15] and of Muehllehner[16,17] have been rotated to permit 360° transverse-section tomographic imaging, and the wire chamber-converter positron camera of Perez-Mendez and co-workers can be used for computed longitudinal tomography.[18] During the past 15 years, beginning with the work of Kuhl, techniques have also been developed for 360° transverse-section imaging of single-gamma radionuclides.[19-24]

2. RING SYSTEMS

2.1 Comparison

In Table I we compare the dimensions, spatial resolution, and sensitivity of three circular positron cameras, the BNL system,[1,2] the UCLA system,[11-13] and our 280-crystal system now under construction.[25,26] The spacing between crystal centers ranges from 30 mm to 10 mm and the resolution FWHM in the reconstructed images is about 75% of this spacing. This is understandable since (a) circular ring systems sample the space at linear intervals of one-half the distance between crystal centers and (b) the sampling theorem states that in order to reliably recover a spatial frequency component, it must be sampled at least twice per cycle. Thus the finest bar pattern that a circular ring system can resolve has a repeat distance approximately equal to the repeat distance of the detectors. Other factors such as (1) the range of positrons in tissue[26-30] and (2) the annihilation angle uncertainty of about 8 mrad FWHM that arises because the positron-electron system does not annihilate at rest[29-32] are less important. For the case of ^{68}Ga *(beta end point 1.9 MeV) in a 100-cm diam ring,* these factors contribute about 3 mm FWHM and 2 mm FWHM, respectively. A higher resolution system with a detector center spacing of 3 mm, for example, might approach a resolution of 3 mm FWHM in transverse section, but only by using the lower-energy positron emitters such as ^{18}F, ^{11}C, or ^{52}Fe.

2.2 The Donner 280-Crystal Positron Ring Camera

We are now constructing a system for the high-resolution imaging of positron-labeled compounds in the human body. This system has been physically simulated by two opposing groups of eight crystals viewing positron-filled phantoms rotated on a turntable between them. See Ref. 26 for details and phantom images. We summarize below some of the properties expected for the full ring, based on measurements made with the 16-crystal system.

a. The spatial resolution is best at the center of the ring, where the point-spread function is circular with 7.5 mm FWHM. At 10 cm from the ring center, the point-spread function is elliptical with 8 mm x 12.5 mm FWHM.

b. The coincident event rate for a 200 μCi point source in air at the center of the ring is 30 000 per sec, including 1700 random coincidences per sec. The coincident event rate for 200 μCi per 1 cm section distributed in a 20 cm cylinder of water is 8600 per sec, including 1400 random coincidences per sec (detection of two unrelated photons within the coincidence resolving time) and 1200 scattered coincidences per sec (detection of two photons from the same positron where one or both have scattered). These random and scattered backgrounds are distributed over a 30-cm field of view and do not present a problem when the activity occupies a small portion of the field.

3. NEW SCINTILLATOR MATERIALS FOR POSITRON COINCIDENCE DETECTION

3.1 Bismuth Germanate ($Bi_4Ge_3O_{12}$)

Recently a new scintillator material (bismuth germanate) has been developed that has several advantages over NaI(Tl) for the detection of annihilation photons[33-35] (Table II). Compared to NaI(Tl), bismuth germanate has a much higher density and atomic number, and thus has a higher gamma-ray detection efficiency. However, bismuth germanate has a much lower scintillation yield than NaI(Tl) and its energy and time resolutions are poorer.[13, 33-35]

Table I. Positron ring systems for transverse section computed tomography.

Institution	BNL	UCLA	Donner (LBL)
References	1,2	11-13	25, 26
Number of Crystals	32	64	280
Crystal face	32 mm diam	20 mm diam	8 mm x 30 mm
Spacing between crystal centers	39 mm	23 mm	10 mm
Image resolution (FWHM of line spread function)	~ 40 mm	17 mm[b]	7.5 mm
Number of projection integrals measured	~ 2 x 270	2 x 864	14 000
Diam of crystal ring	40 cm	47 cm	90 cm
Field of view	~ 30 cm	~ 30 cm	50 cm
Sensitivity (counts/sec/μCi)[a]	240	~ 125[b]	140
Status	imaging in vivo	imaging in vivo	under construction (phantom imaging)

[a]Coincidence rate for a point source in air at the ring center and a 100 keV threshold.
[b]Z. H. Cho (private communication).

Table II. Comparison between NaI (Tl) and $Bi_4Ge_3O_{12}$ crystals.

	NaI (Tl)	$Bi_4Ge_3O_{12}$
Density (g/cm^3)	3.67	7.13[a]
Atomic number	11, 53	83, 32, 8
Relative scintillation output	1.0	0.08[a]
Scintillation peak wavelength (nm)	420	480[a]
Index of refraction at peak wavelength	1.8	2.15[d]
Scintillation decay time (nsec)	230	300[a]
Energy resolution at 662 keV	7% FWHM	15% FWHM[a]
Time resolution[b]	3.4 nsec FWHM	7.1 nsec FWHM
Detection efficiency[c] (20-mm wide crystals)	59% (41%)[d]	90% (88%)
Detection efficiency (8-mm wide crystals)	48% (31%)	82% (80%)
Detection efficiency (4-mm wide crystals)	42% (25%)	72% (70%)

[a]As reported in Ref. 34.
[b]For a 100 keV threshold as reported in Ref. 13.
[c]Calculated detection efficiency for 511 keV photons incident on a bank of rectangular crystals 5 cm deep as shown in Fig. 1. Only single-crystal detections are included.
[d]First percentage: 100 keV threshold on each crystal; percentage in parenthesis: 511 keV threshold.

To determine the relative detection efficiency of NaI(Tl) and $Bi_4Ge_3O_{12}$, we wrote a Monte Carlo computer code that traced the interactions of 511 keV photons through groups of crystals. One crystal was uniformly illuminated along a line across its face by a beam parallel to the 5 cm dimension (Fig. 1). The detection efficiencies given in Table II include only those photons that deposited more than the threshold energy (100 keV or 511 keV) in the illuminated crystal and less than the threshold energy in each of the other crystals.

Using 8-mm wide crystals and a 100 keV threshold, we find that bismuth germanate has a 1.7-fold advantage in detection efficiency over NaI(Tl), and thus a 2.9 fold advantage in coincident detection efficiency. The use of narrower 4-mm wide crystals reduces the efficiencies for both materials by a factor of about 0.88, but the ratio between them remains nearly the same.

The photopeak efficiency for NaI(Tl) is relatively low and photopeak energy selection is generally not used in positron imaging. By comparison, bismuth germanate has a very high photopeak efficiency and when used with a high threshold (300 to 400 keV), would have the advantage of rejecting about half of the tissue-scattered annihilation photons while rejecting very few unscattered photons.

We now estimate the true and accidental event rates for rings of NaI(Tl) and $Bi_4Ge_3O_{12}$ crystals 0.8 x 3 x 5 cm deep. We assume a crystal ring radius c = 40 cm, a shielding slit width S = 2 cm and depth T = 20 cm, and a 200 μCi/cm line source lying on the ring axis in a 20-cm diam cylinder of water (Fig. 2). From Ref. 25 we have:

True unscattered coincident event rate:

$$C_0 = \frac{\omega \mu S^2 c \cdot \mu L_c 2}{4\pi} \quad .$$

Single counting rate:

$$C_s = \frac{\alpha a \varepsilon^2}{f}\left[c e^{-\mu L/2} + \varepsilon_p P_p \right]$$

Accidental event rate[36]:

$$C_a = f C_s^2 \tau / 2 \ ,$$

where α = 200 μCi/cm, a = 37 000 annihilations per sec per μCi, attenuation factor $e^{-\mu L} = 0.15$, and f = the fraction of crystals in coincidence with each crystal = 0.22. This value of f assures that all points within a 30-cm diam circle are sampled at all angles. The estimated values of C_o, C_s, and C_a, as well as the definitions and assumed values of ε, ε_p, P_p, and τ are given in Table III.

In summary, for the positron ring systems of Table III, bismuth germanate has the following advantages over NaI(Tl):

a. For a given amount of activity, the true coincident rate is nearly three times larger and the accidental/true coincidence ratio is nearly two times smaller.

b. For a given accidental/true coincidence ratio, the event rate is about six times larger.

In addition, the reduced penetration of off-axis photons in bismuth germanate provides better spatial resolution toward the edges of the field of view.

3.2 Loaded Organic Scintillators

The ideal scintillator for the coincident detection of annihilation photons would have high density, high atomic number, emit a large number of scintillation photons in a short decay time, operate at room temperature, and be inexpensive. Unfortunately the high-efficiency scintillators such as NaI(Tl), CsI(Na), and $Bi_4(Ge_3O_{12})$, are slow and the fast organic scintillators have low detection efficiency. One notable exception is liquid xenon,[37,38] which has a detection efficiency similar to NaI(Tl) and is about 10 times faster, but requires an operating temperature of about -100°C.

One possibility for an improved scintillator was recently discussed by Lyons,[39] based on work with perylene and bromo-perylene.[40] These compounds are fast organic fluors, whose uv fluorescence is not quenched even by large amounts of iodinated compounds such as 1-iodopropane.

Accordingly, we investigated the light output corresponding to 662 keV Compton electrons for various concentrations of perylene in toluene and for various admixtures of iodinated hydrocarbons. The light output increased with increasing concentration of perylene in toluene and saturated at about 10^{-4} molar. At this concentration the light output increased threefold when argon gas was bubbled through the mixture to de-oxygenate it. The output level reached 70% of pilot B[41] and 20% of NaI(Tl). The output was reduced 5 to 10 fold by only 0.2% admixtures (by volume) of either 1-iodopropane, iodo-

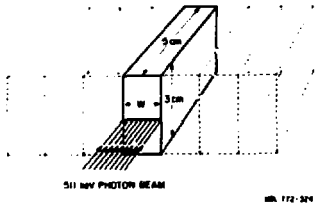

XBL 772-324

Fig. 1. Geometry for Monte Carlo calculation of single-crystal detection efficiency (see Sec. 3.1 and Table II).

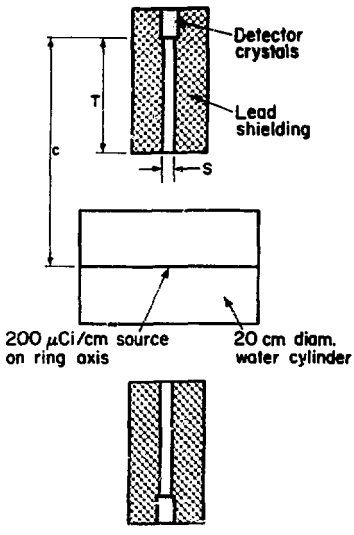

XBL 772-325

Fig. 2. Geometry for calculation of true and accidental coincident event rates using NaI(Tl) and $Bi_4Ge_3O_{12}$ (see Sec. 3.1 and Table III).

Table III. Comparison between NaI(Tl) and $Bi_4Ge_3O_{12}$ crystal rings with 8-mm wide crystals. (see text for details)

Quantity	Symbol	NaI(Tl)	$Bi_4Ge_3O_{12}$
Detection threshold	E_p	100 keV	350 keV
Detection efficiency for 511 keV photons (single-crystal interactions only)	ϵ	0.48	0.80
Probability of a 511 keV photon scattering on passing through 10 cm water and retaining an energy above E_p	P_p	0.6	0.3
Average detection efficiency for above scattered photons	ϵ_p	0.8	0.9
True unscattered coincident event rate	C_o	6400/sec	17 800/sec
Single counting rate (sum over all crystals)	C_s	980 000/sec	850 000/sec
Coincidence resolving time (full width)	τ	15 nsec	30 nsec
Accidental coincident event rate (distributed over a 30 cm field of view)	C_a	1600/sec	2400/sec
Accidental/true coincidence ratio	C_a/C_o	0.25	0.13

methane, diiodomethane, iodoform, or iodobenzene. Larger admixtures reduced the pulse height still further. All the mixtures had strong uv fluorescence. Thus we found (unfortunately) that while iodinated hydrocarbons do not quench perylene for uv excitation, they do quench it for ionizing radiation.

It is hoped that further work in this area will result in a convenient, fast, high-density scintillator.

ACKNOWLEDGMENTS

I am grateful to T.F. Budinger, P. Lyons, and Z.H. Cho for helpful discussions. This work was supported by NCI grant No. RO1 CA-17566-02 and by the United States Energy Research and Development Administration.

REFERENCES

1. S. Rankowitz, J. S. Robertson, W. A. Higinbotham, et al., "Positron Scanner for Locating Brain Tumors," IRE Int. Conv. Rec. 10(9), 49-56 (1962).

2. J. S. Robertson, R. B. Marr, M. Rosenblum, et al., "32 Crystal Positron Transverse Section Detector," in Tomographic Imaging in Nuclear Medicine, pp. 142-155, G. S. Freedman, Ed., Society of Nuclear Medicine, New York, 1973.

3. Special issue on Physical and Mathematical aspects of 3-D image reconstruction, IEEE Trans. Nucl. Sci. NS-21(3) (1974).

4. C. J. Thompson, Y. L. Yamamoto, and E. Meyer, "Reconstruction and Analysis of Data from a Dynamic Positron Imaging Device," J. Nucl. Med. 17, 543 (1976).

5. Y. L. Yamamoto, C. Thompson, and E. Meyer, "Evaluation of Positron Emission Tomography for Study of Cerebral Hemodynamics in a Cross Section of the Head Using Positron Emitting Gallium 68-EDTA and Krypton-77," J. Nucl. Med. 17, 546 (1976).

6. M. M. Ter-Pogossian, M. E. Phelps, E. J. Hoffman, et al., "A Positron-Emission Transaxial Tomograph for Nuclear Imaging (PETT)," Radiology 114, 89-98 (1975).

7. M. E. Phelps, E. J. Hoffman, N. A. Mullani, et al., "Application of Annihilation Coincidence Detection to Transaxial Reconstruction Tomography," J. Nucl. Med. 16, 210-224 (1975).

8. M. E. Phelps, E. J. Hoffman, N. A. Mullani, et al., "Design Considerations for a Positron Emission Transaxial Tomograph (PETT III)," IEEE Trans. Nucl. Sci. NS 23(1), 516-522 (1976).

9. E. J. Hoffman, M. E. Phelps, N. A. Mullani, C. S. Higgins, and M. M. Ter-Pogossian, "Design and Performance Characteristics of a Whole-Body Positron Transaxial Tomograph," J. Nucl. Med. 17, 493-502 (1976).

10. E. J. Hoffman and M. E. Phelps, "An Analysis of Some of the Physical Aspects of Positron Transaxial Tomography, Comput. Biol. Med. 6, 345-360 (1976).

11. Z. H. Cho, L. Eriksson, and J. Chan, "A Circular Ring Transverse Axial Positron Camera," in Workshop on Reconstruction Tomography, M. M. Ter-Pogossian et al., Eds., University Park Press, Baltimore (To be published).

12. Z. H. Cho, J. K. Chan, and L. Eriksson, "Circular Ring Transverse Axial Positron Camera for 3-Dimensional Reconstruction of Radionuclides Distribution," IEEE Trans. Nucl. Sci. NS23(1), 613-622 (1976).

13. Z. H. Cho, J. Eriksson, M. Singh, et al., "Performance and Evaluation of the Circular Ring Transverse Axial Positron Camera (CRTAPC)," IEEE Trans. Nucl. Sci. NS24(1),532-543(1977).

14. G. L. Brownell, C. A. Burnham, D. A. Chesler, et al., "Transverse Section Imaging of Radionuclide Distributions in Heart, Lung, and Brain," in Workshop on Reconstruction Tomography," M. M. Ter-Pogossian et al., Eds., University Park Press, Baltimore (to be published).

15. J. A. Correia, D. A. Chesler, B. Hoop Jr., et al., "Transverse Section Reconstruction with Positron Emitters and the MGH Positron Camera," J. Nucl. Med. 17, 551 (1976).

16. G. Muehllehner, "Positron Camera with Extended Counting Rate Capability," J. Nucl. Med. 16, 653-657 (1975).

17. G. Muehllehner, M. P. Buchin, and J. H. Dudek, "Performance Parameters of a Positron Imaging Camera" IEEE Trans. Nucl. Sci. NS23(1), 528-537 (1976).

18. L. T. Chang, B. Macdonald, and V. Perez-Mendez, "Axial Tomography and Three Dimensional Image Reconstruction," IEEE Trans. Nucl. Sci. NS23(1), 568-572 (1976).

19. D. E. Kuhl and R. Q. Edwards, "Image Separation Radioisotope Scanning," Radiology 80, 653 (1963).

20. D. E. Kuhl and R. Q. Edwards, "The Mark III Scanner: A Compact Device for Multiple-View and Section Scanning of the Brain," Radiology 96, 563-570 (1970).

21. T. F. Budinger and G. T. Gullberg, "Transverse Section Reconstruction of Gamma-ray Emitting Radionuclides in Patients," in Workshop on Reconstruction Tomography, M. M. Ter-Pogossian et al., Eds., University Park Press, Baltimore (to be published).

22. J. W. Keyes, N. Orlandea, W. J. Heetderks, and P. F. Leonard, "The Humongotron-A Gamma Camera Transaxial Tomograph," J. Nucl. Med. 17, 552 (1976).

23. R. Jaszczak, D. Huard, P. Murphy, and J. Burdine, "Radionuclide Emission Computed Tomography with a Scintillation Camera," J. Nucl. Med. 17, 551 (1976).

24. T. F. Budinger, S. E. Derenzo, G. T. Gullberg, W. L. Greenberg, and R. H. Huesman, "Emission Computer Assisted Tomography with Single-Photon and Positron Annihilation Photon Emitters," J. Comput. Assisted Tomography 1 (1977) (in press).

25. S. E. Derenzo, H. Zaklad, and T. F. Budinger, "Analytical Study of a High-Resolution Positron Ring Detector System for Transaxial Reconstruction Tomography," J. Nucl. Med. 16, 1166-1173 (1975).

26. S. E. Derenzo, T. F. Budinger, J. L. Cahoon, R. H. Huesman, and H. G. Jackson, "High Resolution Computed Tomography of Positron Emitters," IEEE Trans. Nucl. Sci., NS24(1), 544-558 (1977).

27. M. E. Phelps, E. J. Hoffman, S. C. Huang, et al., "Effect of Positron Range on Spatial Resolution," J. Nucl. Med. 16, 649-652 (1975).

28. Z. H. Cho, J. K. Chan, L. Eriksson, et al., "Positron Ranges Obtained from Biomedically Important Positron-Emitting Radionuclides," J. Nucl. Med. 16, 1174-1176 (1975).

29. G. Muehllehner, "Resolution Limit of Positron Cameras," J. Nucl. Med. 17, 757 (1976).

30. S. E. Derenzo and T. F. Budinger, "Resolution Limit for Positron Imaging Devices," J. Nucl. Med. (letter in press).

31. A. T. Stewart, "Momentum Distribution of Metallic Elutions by Positron Annihilation," Can. J. Phys. 35, 168-183 (1957).

32. P. Colombino, B. Fiscella, and L. Trossi, "Study of Positronium in Water and Ice from 22 to -144°C by Annihilation Quantum Measurements," Nuovo Cimento 38, 707-723 (1965).

33. M. J. Weber and R. R. Monchamp, "Luminescence of $Bi_4Ge_3O_{12}$: Spectral and Decay Properties," J. Appl. Phys. 44, 5495-5499 (1973).

34. O. H. Nestor and C. Y. Huang, "Bismuth Germanate: A High-Z Gamma Ray and Charged Particle Detector," IEEE Trans. Nucl. Sci. NS22(1), 68-71 (1975).

35. Z. H. Cho and M. R. Farukhi, "New Bismuth Germanate Scintillation Crystal - A Potential Detector for the Positron Camera Applications," J. Nucl. Med. (to be published).

36. In Ref. 25 the factor 1/2 was omitted.

37. J. A. Northrop, J. M. Gursky, and A. E. Johnsrud, "Further Work with Noble Element Scintillators," IRE Trans. Nucl. Sci. NS 5(3), 81-87 (1958).

38. L. Lavoie, "Liquid Xenon Scintillators for Imaging of Positron Emitters," Med. Phys. 3, 283-293 (1976).

39. P. Lyons, Technology Update on Fast Plastic Scintillators for Medical Applications, IEEE Trans. Nucl. Sci. NS24, this volume (1977).

40. H. Dreeskamp, E. Koch, and M. Zander, "Fluorescence of Bromoperylenes and the Requirements of Heavy-Atom Quenching," Chem. Phys. Lett. 31, 251-253 (1975).

41. Manufactured by Nuclear Enterprises Inc., San Carlos, CA.